ISSN 1674-1056
http://cpb.iphy.ac.cn
http://iopscience.iop.org/cpb
中国物理 B
Chinese Physics
中国物理 Chinese Physics B

Improvement of 2.79-μm laser performance on laser diode side-pumped GYSGG/Er,Pr:GYSGG bonding rod with concave end-faces

Xu-Yao Zhao(赵绪尧)[1,2], Dun-Lu Sun(孙敦陆)[1], Jian-Qiao Luo(罗建乔)[1], Hui-Li Zhang(张会丽)[1], Zhong-Qing Fang(方忠庆)[1,2], Cong Quan(权聪)[1,2], Lun-Zhen Hu(胡伦珍)[1,2], Zhi-Yuan Han(韩志远)[1,2], Mao-Jie Cheng(程毛杰)[1], Shao-Tang Yin(殷绍唐)[1]

Citation: Chin. Phys. B . 2019, 28(11): 114208 . **doi:** 10.1088/1674-1056/ab4ce0
Journal homepage: http://cpb.iphy.ac.cn; http://iopscience.iop.org/cpb

What follows is a list of articles you may be interested in

Non-crossover sub-Doppler DAVLL in selective reflection scheme

Lin-Jie Zhang(张临杰), Hao Zhang(张好), Yan-Ting Zhao(赵延霆), Lian-Tuan Xiao(肖连团), Suo-Tang Jia(贾锁堂)
Chin. Phys. B . 2019, 28(8): 084211 . **doi:** 10.1088/1674-1056/28/8/084211

Active hyperspectral imaging with a supercontinuum laser source in the dark

Zhongyuan Guo(郭中源), Yu Liu(刘煜), Xin Zheng(郑鑫), Ke Yin(殷科)
Chin. Phys. B . 2019, 28(3): 034206 . **doi:** 10.1088/1674-1056/28/3/034206

Nonlinear behavior of the population dynamics of three-level systems in the presence of single photon absorption

Allam Srinivasa Rao
Chin. Phys. B . 2019, 28(2): 024211 . **doi:** 10.1088/1674-1056/28/2/024211

Laser absorption spectroscopy for high temperature H_2O time-history measurement at 2.55 μm during oxidation of hydrogen

Yu-Dan Gou(苟于单), De-Xiang Zhang(张德翔), Yi-Jun Wang(王易君), Chang-Hua Zhang(张昌华), Ping Li(李萍), Xiang-Yuan Li(李象远)
Chin. Phys. B . 2018, 27(7): 074213 . **doi:** 10.1088/1674-1056/27/7/074213

Analysis of algebraic reconstruction technique for accurate imaging of gas temperature and concentration based on tunable diode laser absorption spectroscopy

Hui-Hui Xia(夏晖晖), Rui-Feng Kan(阚瑞峰), Jian-Guo Liu(刘建国), Zhen-Yu Xu(许振宇), Ya-Bai He(何亚柏)
Chin. Phys. B . 2016, 25(6): 064205 . **doi:** 10.1088/1674-1056/25/6/064205

Improvement of 2.79-μm laser performance on laser diode side-pumped GYSGG/Er,Pr:GYSGG bonding rod with concave end-faces*

Xu-Yao Zhao(赵绪尧)[1,2], Dun-Lu Sun(孙敦陆)[1,†], Jian-Qiao Luo(罗建乔)[1], Hui-Li Zhang(张会丽)[1], Zhong-Qing Fang(方忠庆)[1,2], Cong Quan(权聪)[1,2], Lun-Zhen Hu(胡伦珍)[1,2], Zhi-Yuan Han(韩志远)[1,2], Mao-Jie Cheng(程毛杰)[1], and Shao-Tang Yin(殷绍唐)[1]

[1] *The Key Laboratory of Photonic Devices and Materials, Anhui Province, Anhui Institute of Optics and Fine Mechanics, Chinese Academy of Sciences, Hefei* 230031, *China*

[2] *University of Science and Technology of China, Hefei* 230022, *China*

(Received 27 June 2019; revised manuscript received 28 September 2019; published online 30 October 2019)

A comparative study on the laser performance between bonding and non-bonding Er,Pr:GYSGG rods side-pumped by 970-nm laser diodes (LDs) is conducted for the thermal lensing compensation. The analyses of the thermal distribution and thermal focal length show that the bonding rod possesses a high cooling efficiency and weak thermal lensing effect compared with the conventional Er,Pr:GYSGG rod. Moreover, the laser characteristics of maximum output power, slope efficiency, and laser beam quality of the bonding rod with concave end-faces operated at 2.79 μm are improved under the high-repetition-rate operation. A maximum output power of 13.96 W is achieved at 150-Hz and 200-μs pulse width, corresponding to a slope efficiency of 17.7% and an electrical-to-optical efficiency of 12.9%. All results suggest that the combination of thermal bonding and concave end-face is a suitable structure for thermal lensing compensation.

Keywords: laser performance, GYSGG/Er,Pr:GYSGG bonding rod, thermal lensing compensation, concave end-faces

PACS: 42.62.Fi, 42.70.Hj, 68.60.Dv, 81.65.Ps **DOI:** 10.1088/1674-1056/ab4ce0

1. Introduction

Compact and reliable Er-doped solid-state lasers in a strong water absorption range of 2.7 μm–3 μm enable their potential operation in medicine, atmospheric sounding, ranging (lidar), *etc*. Now, it is of particular significance to utilize this wavelength laser with a high repetition rate in the fields of laser surgery and optoelectronic countermeasure. Moreover, the 2.7-μm–3-μm lasers can be used as a suitable pumping source for an optical parametric oscillator (OPO) to generate 3.8-μm–12.4-μm mid-infrared lasers.[1] An Er^{3+}-doped garnet-host $Gd_{1.17}Y_{1.83}Sc_2Ga_3O_{12}$ (GYSGG) crystal has advantages in 2.79-μm laser operation due to its relatively high thermal conductivity, excellent mechanical strength, and radiation-resistant ability,[2] but the unfavorable lifetime ratio between the upper $^4I_{11/2}$ and lower $^4I_{13/2}$ level has a serious effect on the laser threshold and efficiency. Based on highly Er-doped laser system, although energy recycling by energy transfer upconversion (ETU) can allow continuous-wave (CW) laser to operate, the multiphoton relaxation following the ETU processes leads large heat to produce.[3] Therefore, thermal stress and strain appear inside the gain medium, which in turn influence the laser output characteristic. As an alternative, an Er:GYSGG crystal depopulated with Pr^{3+} has exhibited a better laser performance by deactivating the lower level.[4,5] The high average power of 8.86 W at 125-Hz and 200-μs pulse width has already been achieved by using a laser diode (LD) side-pumped scheme.[6]

However, the main problem that limits the pulse energy scaling up to an even higher level for Er,Pr:GYSGG crystal, is the generation of heat inside the crystal under high pump power. Steep temperature gradient inside the crystal results in serious thermal distortion and surface bending, which limits the further improvement of the high-repetition-rate laser at the 2.79-μm wavelength. Since thermal lensing effect cannot be avoided under high pump power, many efforts have already been devoted to compensating for reducing the thermal lensing effect, such as incorporating additional intracavity elements,[7] designing resonant cavity structures,[8] *etc*. However, the most common approaches to direct compensation in an active medium are thermal bonding on the end-face of the crystal[9] and grinding negative curvatures on the crystal ends.[10] A composite formation of bonding rod with undoped crystal as the end-cap offers a suitable cooling structure to reduce the temperature in an active segment and thermally induced stress. The improvement effect of thermal diffusion is significant to compensate for the thermal lens magnitude and

*Project supported by the National Natural Science Foundation of China (Grant Nos. 51872290, 51702322, and 51802307) and the National Key Research and Development Program of China (Grant No. 2016YFB1102301).

†Corresponding author. E-mail: dlsun@aiofm.ac.cn

© 2019 Chinese Physical Society and IOP Publishing Ltd

improve the laser performance. In another approach, grinding the crystal end-faces with negative curvature can increase laser beam mode volume and negate the positive lensing of the crystal without inserting any optical element. There are only a few reports on the extension of concave end-face to the bonding rod and the detailed analysis of its lasing characteristics. In this work, the thermal bonding and concave end-face are combined on the Er,Pr:GYSGG rod to depress the thermal lensing effect and further improve the laser performance.

Here in this work we demonstrate a comparative study on the laser performance between bonding and non-bonding Er,Pr:GYSGG rods side-pumped by 970-nm LDs. The thermal induced temperature distribution of the bonding rod is theoretically simulated in comparison with the conventional Er,Pr:GYSGG rod, and the thermal focal length and laser characteristics are measured to analyze the effects of thermal bonding and concave end-faces on thermal lensing compensation.

2. Experimental setup

An Er,Pr:GYSGG crystal with dopant containing 18-at.% Er^{3+} and 0.2-at.% Pr^{3+} was grown by the Cz method.[6] The dimensions of Er,Pr:GYSGG crystal rods were processed into Φ3 mm×85 mm and Φ3 mm×55 mm, respectively. Pure GYSGG crystal rods (Φ3 mm×15 mm) were bonded thermally together with Er,Pr:GYSGG rod (Φ3 mm ×55 mm) at 1200 °C for 10 h. Both end-faces of the crystal rods were optically polished and coated with an antireflection film near 2.79 μm. The flat-flat Er,Pr:GYSGG and GYSGG/Er,Pr:GYSGG bonding rods were marked as a-GYSGG and b-GYSGG for simplicity, respectively, and the concave–concave GYSGG/Er,Pr:GYSGG bonding rod with a negative curvature of 500 mm was denoted as c-GYSGG. The experimental setup with a plane-parallel resonator cavity was designed as schematically shown in Fig. 1. The side-pumped source (CEO-RBAT35-3P200) utilizes three radial LD arrays to directly excite the solid-state laser medium at a central wavelength of 970 nm (full wavelength at half maximum (FWHM) value = 4.6 nm). The effective pump length and water-cooling length of rod were about 50 mm and 70 mm, respectively. Compared with the LD end-pumped and flash pumped configurations, the side-pump geometry has excellent gain uniformity. The available maximum current and pulse width were 150 A and 200 μs, respectively. The laser system was maintained at a temperature of 22 ±0.1 °C by cooling water circulation. The input mirror (M1) was high-reflection coated at 2.79 μm, and the output coupler mirrors (M2) with transmissions of 10%, 15%, and 20% at 2.79 μm were used. The positions of the M1 and M2 were carefully adjusted to being strictly symmetrical for the crystal rods. The laser output power was measured by a power meter (OPHIR 30 A-BB-18). The laser beam profile and M^2 factor were recorded with a pyroelectric array camera (Ophir-Spiricon PY-III-HR).

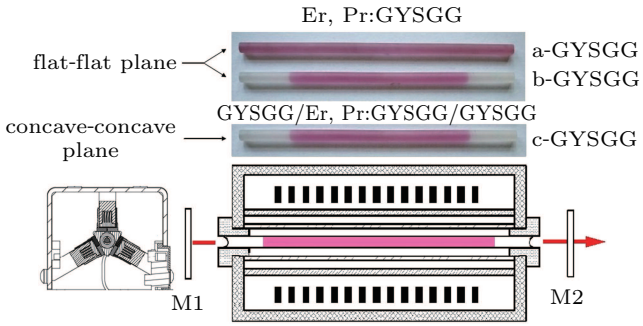


Fig. 1. Schematic diagram of GYSGG/Er,Pr:GYSGG bonding rod with concave end-faces pumped by 970-nm LD arrays.

3. Results and discussion

3.1. Temperature distribution

When the pump power is very high, a significant portion of the pump light is converted into heat inside the laser material. Apart from concentration quenching, excited state absorption and upconversion, it originates mainly from the quantum defect and inherent optical absorption of the laser gain medium.[11] By conduction through the coolant, heat extraction from rod center to rod surface leads to a nonuniform temperature distribution in the crystal rod, which in turn causes thermal lensing effect and thus affects the laser output. Consequently, it is significant to discuss the temperature distribution inside the crystal rod. Under the assumption of uniform internal heat generation and the small variation of coolant temperature at the axial direction, the analytical treatment of heat conduction in an isotropic medium can be described by[12]

$$\rho c_P \frac{\partial T}{\partial t} = \nabla \cdot (k(T) \cdot \nabla T) + Q, \tag{1}$$

where Q is the heat intensity, ρ is the density, c_P is the specific heat at constant pressure, k is the thermal conductivity, and ∇ denotes the gradient operator. Under the steady-state condition, if we assume k to be constant and the heat flow is regarded as being strictly radial and axial, then the temperature is a function of radial (r) and longitudinal (z), so the heat conduction equation (1) becomes

$$\nabla^2 T = \frac{\partial^2 T}{\partial r^2} + \frac{1}{r}\frac{\partial T}{\partial r} + \frac{\partial^2 T}{\partial z^2} = -\frac{Q}{k}. \tag{2}$$

The boundary condition of the cylindrical rod surface and the coolant is set below, according to Newton's law of heat transfer

$$k \cdot \left.\frac{\partial T}{\partial n}\right|_{\text{Surf}} = h \cdot (T_{\text{C}} - T|_{\text{Surf}}), \tag{3}$$

where h is the heat transfer coefficient, T_{C} is the coolant temperature, and n is the normal to the surface.

Figure 2 shows the simulated relative temperature distribution and center temperature at the cross-section of the bonding surfaces in the two crystal rods. The temperature distributions of the LD homogeneously side-pumped two crystal rods are simulated by using the COMSOL Multiphysics software. With the use of trigonal symmetric LD arrays, the pumping intensity distribution on the effective pumped portion of the crystal rod (50 mm) is approximately uniform. The optimal total length of the laser rod is about 85 mm, so the 55-mm-long Er,Pr:GYSGG crystal is chosen for fully being pumped and the two 15-mm-long pure GYSGG crystal rods are selected for compensating for the thermal effect. In this calculation, 85 W of pump power at 125-Hz and 200-μs pulse width is assumed to be fully converted into the heat density of 200 W/cm^3 in active segment. The relevant parameters used for numerically calculating the temperature profile of the crystal rod are listed in Table 1.[13] At the cross-section of the bonding surface and corresponding position, the maximum center temperature and radial temperature gradient for each of the GYSGG/Er,Pr:GYSGG bonding rods (312.5 K) are lower than those of conventional a-GYSGG (314.7 K), and their difference value rises with the increase of heat density. This phenomenon indicates that the heat generated in a-GYSGG can be effectively transfer to the undoped GYSGG end caps, which displays a better cooling efficiency due to the higher thermal conductivity of GYSGG crystal. Therefore, the bonding rod will weaken thermal lensing effect by attenuating the temperature gradient. In the following subsections, a detailed analysis is performed on the laser properties by use of the bonding rods.

Table 1. Parameters used in numerical simulation.

Parameter	Value	Parameter	Value
Q	200 W/cm^3	T_C	295.15 K
h_1 (in water)	1 W/cm^2·K	h_2 (in air)	0.05 W/cm^2·K
k_1 (Er,Pr:GYSGG)	4.663 W/(m·K)	k_2 (GYSGG)	6 W/(m·K)

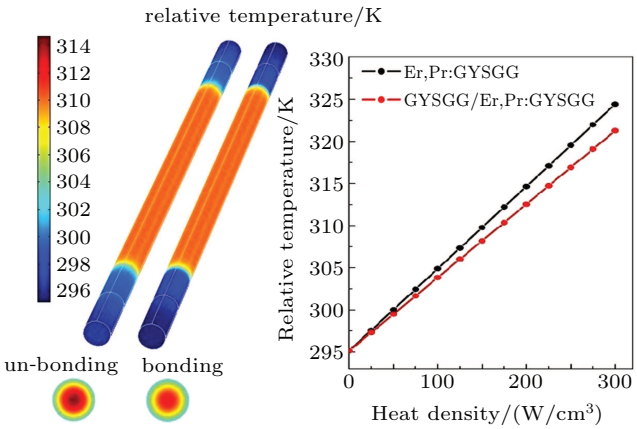


Fig. 2. Relative temperature distribution and center temperature at cross-section of bonding surfaces in two crystal rods.

3.2. Thermal focal length

The thermal lensing effect mainly results from the refractive index and stress-dependent variations and end-surface expansion by the temperature gradient that is often expressed by thermal focal length.[14] Complete compensation for this effect is difficult, because the rod acts as a convergent lens with variable focal lengths under the different values of pump power. In order to investigate the effects of the thermal bonding and concave end-faces on the thermal lensing effect, the thermal focal length for each of the three laser rods at 125-Hz and 200-μs pulse width is measured by a simple technique, which was described in our previous work.[6] The thermal focal lengths grow in inverse proportion to LD input power as shown in Fig. 3. The thermal focal lengths of the bonding rods are all larger than that of a-GYSGG at the same input power. When the pump power is increased up to a maximum input power of 85 W, the focal length of a-GYSGG is almost 200 mm, while those of b-GYSGG and c-GYSGG are close to 240 mm and 280 mm, respectively. And the maximum focal lengths of 500 mm are achieved to be about 67.9 W, 71.8 W, and 74.9 W for a-GYSGG, b-GYSGG, and c-GYSGG, respectively. In comparison of the thermal focal lengths of the three crystal rods, it turns out that the thermal bonding with undoped GYSGG crystals is impactful for compensating for the thermal lensing, which can be attributed to the reduction of the temperature gradient. Furthermore, the combination of the thermal bonding and concave end-faces in c-GYSGG has more advantage in offsetting the thermal lensing than the flat-flat b-GYSGG, because the concave surfaces service as a diverging optical component to negate the positive lensing of the rods.

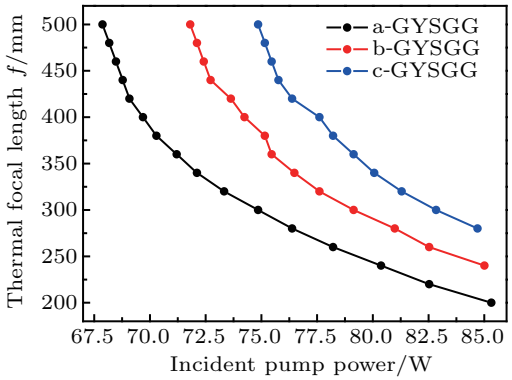


Fig. 3. Thermal focal lengths *versus* input power for three different crystals.

3.3. Lasing characteristics

As mentioned in Subsections 3.1 and 3.2, the bonding rod is beneficial for compensating for the thermal lensing effect. Then the improvement of laser performance of the bonding rod is expected to be effective under the same experimental condition in contrast with the conventional a-GYSGG. Here we analyze the characteristics of the maximum output power,

slope efficiency, and laser beam quality (M^2 factor) by taking into account the different structures of the bonding rods. In order to achieve the optimal laser outputs for the three laser rods, the effects of the cavity length on the average output power under different frequencies and pulse widths with the same M2 (T = 10%, 15%, and 20%) and current (150 A) are further explored as shown in Fig. 4. It can be noted that the laser characteristics are significantly different from those of the different types of laser crystal rods though they are in the same pump mode.

It can be observed in Fig. 4 that the average output power strongly depends on the cavity length, and the optimal cavity length of a-GYSGG significantly differs from that of the bonding rods. In the low-frequency pump mode, the laser rod has a weaker thermal lensing effect. The average output power increases with the decrease of cavity length at 50-Hz repetition rate for each of all three laser rods, because the diffraction loss decreases in shorter cavity. As the frequency increases, there exists a growing thermal lensing effect in the active segment of the laser rod, which will result in the mismatching of pump light to cavity mode and the instability of plane parallel resonator.[15] This means that the optimal cavity length dynamically changes with the pump power because of the thermal lensing effect. The largest average output power values in the cases of a cavity length of 170 nm for a-GYSGG and 150 mm for b-GYSGG in the high-frequency pump mode are obtained, and the obtained largest average output power values of c-GYSGG are achieved with the cavity lengths of less than 150 mm. The shorter optimal cavity lengths in the bonding rods are attributed to the lower thermal lensing effect, which is beneficial to the increase of the resonator stability and the improvement of the maximum output power. Therefore, the average output power of a-GYSGG decreases in the high-frequency pump mode after reaching saturation, but that of the bonding rods almost maintains the same level as the maximum.

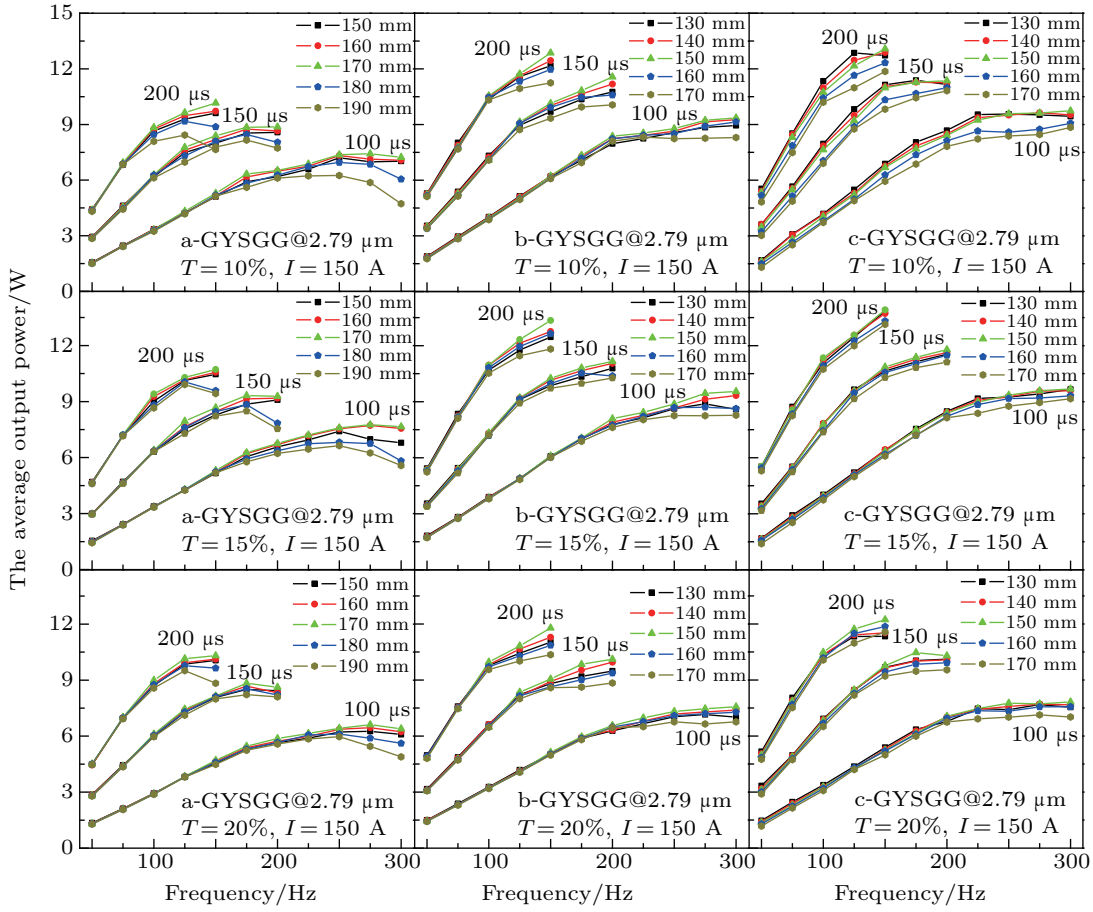


Fig. 4. Plots of average output power *versus* frequency for different pulse widths, different output coupler mirror transmissions, and cavity lengths.

Figure 5 presents the maximum output powers of three laser rods with the different cavity lengths and M2 (T = 10%, 15%, and 20%), which are all operated at 150-Hz and 200-μs pulse width. The behaviors of maximum output powers are almost identical in all three laser rods. The M2 with a 15% transmission generates larger average output power than other M2s with transmission values of 10% and 20%, respectively, under the same experimental condition, which is independent of the type of laser crystal rod and cavity length. With a cavity length of 170 mm and 15% M2, a maximum output power value of 10.72 W is obtained in a-GYSGG at a pump power value of 115 W. In contrast, maximum output power values of

13.35 W and 13.96 W correspond to those of the bonding rods of b-GYSGG and c-GYSGG with a cavity length of 150 mm, which are approximately 24.5% and 30.1% higher than that of a-GYSGG. Meanwhile, the E–O efficiency can be calculated from the following equation:

$$\eta = \frac{P_{\text{output}}}{P_{\text{pump}}}, \tag{4}$$

where η is the E–O efficiency, P_{output} is the average output power, and P_{pump} is the pump power. The E–O efficiency of a-GYSGG, b-GYSGG, and c-GYSGG at 150 Hz are 9.9%, 12.4%, and 12.9%, respectively. The maximum output power with a cavity length of 170 mm is far less than that with an optimal cavity length of 150 mm for the bonding rods. The comparative results clearly indicate that the bonding rods can significantly improve the output performance at high pump power, and the concave end-faces can further compensate for thermal lensing effect by reducing the diffraction loss. In our previous work,[6] a maximum output power value of 8.86 W at 125-Hz and 200-μs pulse width was achieved in a-GYSGG. The increasing of maximum output power is due to the fact that the 970-nm LD in this work matches the absorption peak of Er,Pr:GYSGG crystal better than 966-nm LD in previous work.

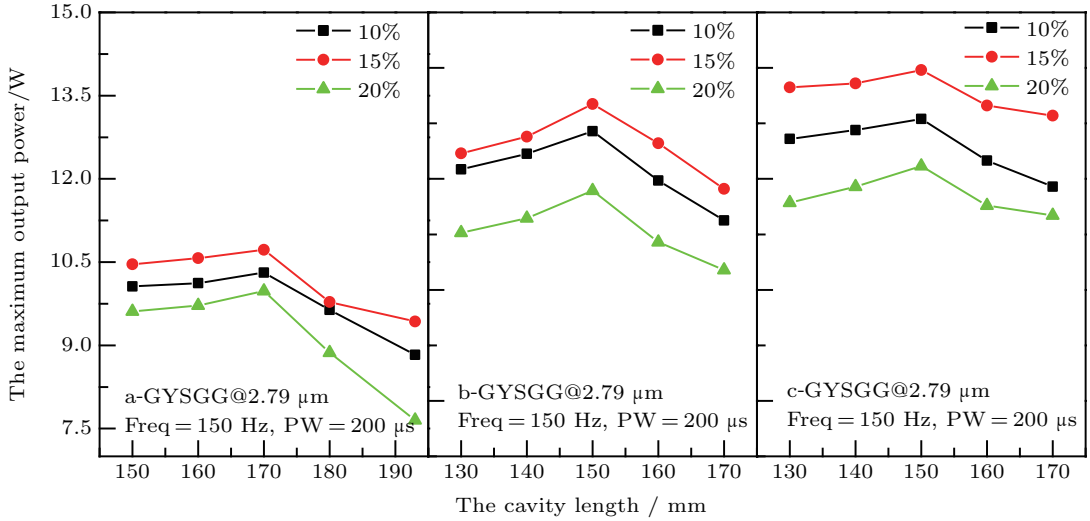


Fig. 5. Plots of maximum output power *versus* cavity length for different transmission values. In the figure, the abbreviation Freq is used for frequency, PW for pulse width.

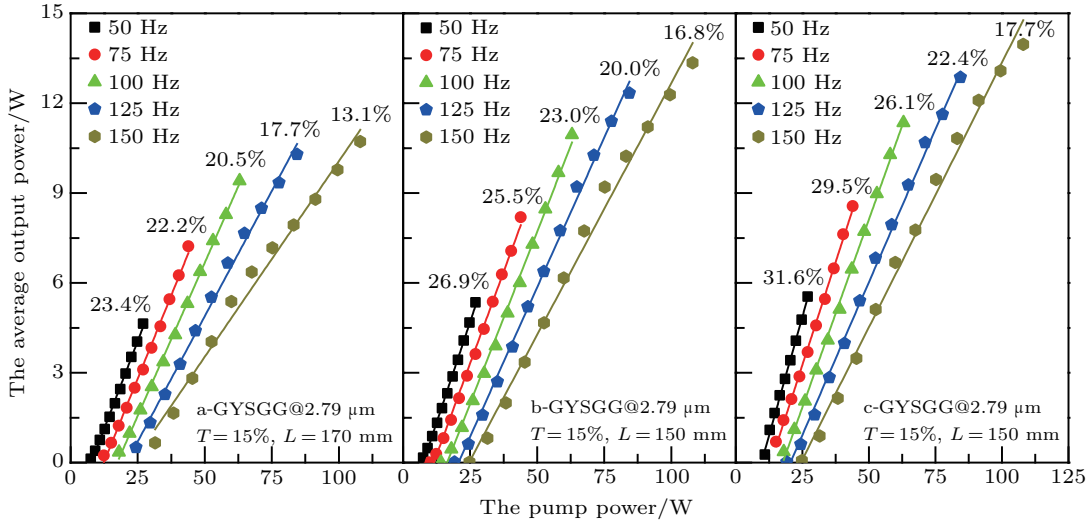


Fig. 6. Plots of average output power *versus* input power at different frequencies.

Figure 6 shows the input–output characteristics of three laser rods at a pulse width of 200 μs, which are obtained with the 15% M2 and optimal cavity length. The average output power increases approximately linearly with input power increasing, but the actual maximum output power at low repetition rate cannot reach the saturation value for the limitation of maximum working current (150 A). Notably, the slope efficiency decreases with repetition rate increasing, which is attributed to the fact that the increase of pump energy in a high-frequency mode leads to more heat generation and stronger thermal lensing effect. The slope efficiency of a-GYSGG, b-GYSGG, and c-GYSGG at 50 Hz are linearly fitted by 23.4%,

26.9%, and 31.6%, respectively, and these of three laser rods at 150 Hz are reduced by 13.1%, 16.8%, and 17.7%. With the exception of the improvement of maximum output power in bonding rods mentioned above, the slope efficiencies of b-GYSGG and c-GYSGG at different frequencies each have an obvious increase compared with that of a-GYSGG due to low thermal lensing effect. In contrast, the slope efficiencies of b-GYSGG at different frequencies are about 3% higher than that of a-GYSGG. But the slope efficiency of c-GYSGG in a low-frequency mode increases more than in high-frequency mode, which contributes to the increase of threshold caused by concave end-faces of c-GYSGG. This is believed to be due to the fact that the thermal lensing effect is weaker under low pump power, so concave end-faces do not fulfil the function of thermal lensing compensation. Then concave end-face will act as a concave lens to increase the diffraction losses of laser oscillation, which results in a higher threshold.

The M^2 factor of the output laser beams, operated at 150-Hz and 200-μs pulse width, at the pump power up to 108 W are determined by the camera with a 400-mm focal length K9 lens. The laser beam radius at the maximum output power is recorded at the position around the K9 lens focus point, and a hyperbolic shape is adopted to fit the experimental data as shown in Fig. 7. The quality factor M^2 is calculated from the following equation:[16]

$$M^2 = \frac{\omega\Theta\pi}{4\lambda}, \tag{5}$$

where ω is the beam waist diameter, Θ is the far-field divergence, and λ is the wavelength. The value of laser beam quality factor M^2 of a-GYSGG, b-GYSGG, and c-GYSGG in the x and y direction are extracted to be 3.96/3.99, 3.74/3.76, and 3.41/3.39, respectively. The reduction in M^2 factor means the reduction of laser mode. The two bonding rods show a smaller M^2 factor than a-GYSGG, which means that the bonding rods can acquire a better laser beam quality besides the improvement of maximum output power and slope efficiency. In addition, c-GYSGG gives a smaller M^2 factor than b-GYSGG, because the concave end-faces can increase laser beam mode volume.

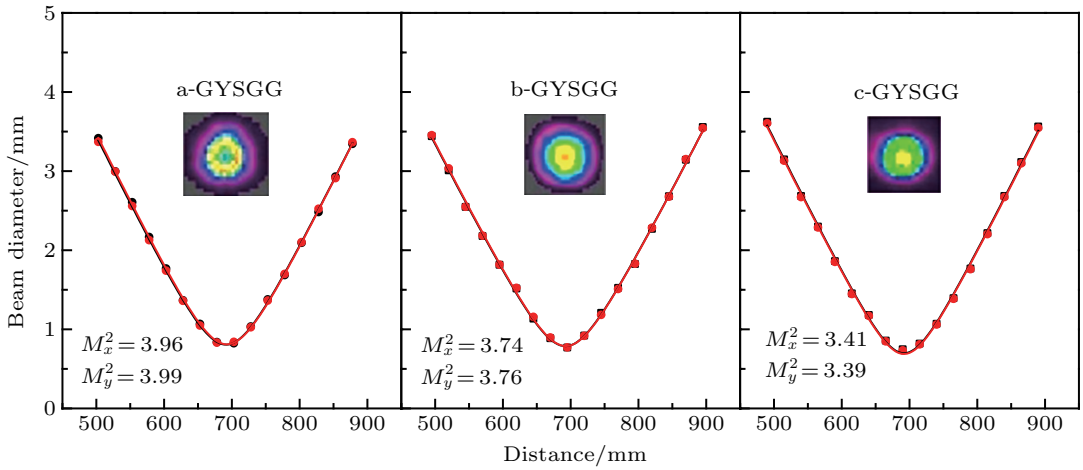


Fig. 7. Plots of laser beam diameter *versus* propagation distance, with insert showing beam profiles under pump power of 108 W.

A comparative study of the laser characteristics among a-GYSGG, b-GYSGG, and c-GYSGG shows that the improvement of the laser characteristics is essentially in agreement with the behavior of thermal focal lengths measured in Fig. 3. The undoped end-caps of bonding rods conduce to the decrease of the thermal distortion in the active segment of laser rods, and the concave end-faces can further suppress thermal lensing effect at high pump power. Therefore, the c-GYSGG exhibits a 2.79-μm mid-infrared laser with high power, high efficiency, and good beam quality by compensating for thermal lensing effect. The combination of thermal bonding and concave end-faces brings an extraordinary improvement in the laser performance of the LD side-pumped Er,Pr:GYSGG rod.

4. Conclusions

In this work, we demonstrate the compensation for strong thermal lensing effect for the LD side-pumped GYSGG/Er,Pr:GYSGG bonding rod in order to improve the laser performance operated at the 2.79 μm. Comparative studies on the basic laser characteristics between bonding and non-bonding Er,Pr:GYSGG rods are performed. The simulated temperature distributions reveal a better cooling efficiency of the undoped GYSGG end-caps, which is beneficial to the decrease of the temperature gradient and compensating for the thermal lensing effect. Meanwhile, the concave end-faces have also advantage in inhibiting the thermal lensing to obtain 2.79-μm laser with higher maximum output power and slope efficiency. At 150-Hz and 200-μs pulse

width, a maximum output power of 13.96 W is achieved in the GYSGG/Er,Pr:GYSGG bonding rod with concave end-faces, corresponding to the slope efficiency of 17.7% and E–O efficiency of 12.9%, and is approximately 30% higher than that in a conventional non-bonding rod. The reduction of M^2 factor further indicates that the bonding rods can enhance the laser beam quality under the high pump power. All results confirm that the GYSGG/Er,Pr:GYSGG bonding rod with concave end-faces possesses an effective compensation for the thermal lensing effect, which is suitable to the operation at high power and high repetition rate.

References

[1] Vodopyanov K L, Ganikhanov F, Maffetone J P, Zwieback I and Ruderman W 2000 *Opt. Lett.* **25** 841

[2] Chen J K, Sun D L, Luo J Q, Xiao J Z Dou R Q and Zhang Q L 2013 *Opt. Commun.* **301–302** 84

[3] Pollnau M and Jackson S D 2001 *IEEE J. Quantum Electron.* **7** 30

[4] Chen J K, Sun D L, Luo J Q, Zhang H L, Dou R Q, Xiao J Z, Zhang Q L and Yin S T 2013 *Opt. Express* **21** 23425

[5] Zhao X Y, Sun D L, Luo J Q, Zhang H L, Fang Z Q, Quan C, Li X L, Cheng M J, Zhang Q L and Yin S T 2017 *Chin. Phys. B* **26** 074217

[6] Zhao X Y, Sun D L, Luo J Q, Zhang H L, Fang Z Q, Quan C, Hu L Z, Cheng M J, Zhang Q L and Yin S T 2018 *Opt. Lett.* **43** 4312

[7] Neuenschwander B, Weber R and Weber H P 1995 *IEEE J. Quantum Electron.* **31** 1082

[8] Hajiesmaeilbaigi F, Razzaghi H, Esfahani M M, Moghaddam M R A and Sabbaghzadeh J 2005 *Laser Phys. Lett.* **2** 437

[9] Tsunekane M, Taguchi N and Inaba H 1998 *Appl. Opt.* **37** 5713

[10] Wang J T, Cheng T Q, Wang L, Yang J W, Sun D L, Yin S T, Wu X Y and Jiang H H 2015 *Laser Phys. Lett.* **12** 105004

[11] Weber R, Neuenschwander B, Weber H P 1999 *Opt. Mater.* **11** 245

[12] Brown D C 1997 *IEEE J. Quantun. Electron.* **33** 861

[13] Fang Z Q, Sun D L, Luo J Q, Zhang H L, Zhao X Y, Quan C, Hu L Z, Cheng M J, Zhang Q L and Yin S T 2017 *Opt. Express* **25** 21349

[14] Koechner W 2005 *Solid State Laser Engineering* (Berlin: Springer) Chap. 7

[15] Degallaix J, Slagmolen B, Zhao C, Ju L and Blair D 2005 *Gen. Relativ. Gravit.* **37** 1581

[16] Siengman A E 1993 *Defining And Measuring Laser Beam Quality In Solid State Lasers* (New York: Plenum) p. 13